Title

Organization of the sleep-related neural systems in the brain of the harbour porpoise (Phocoena phocoena)

Journal

The Journal of Comparative Neurology, 524(10)

ISSN

1550-7149

Authors

Dell, Leigh-Anne
Patzke, Nina
Spocter, Muhammad A
et al.

Publication Date

2016-07-01

DOI

10.1002/cne.23929

Peer reviewed

HHS Public Access

Author manuscript

J Comp Neurol. Author manuscript; available in PMC 2022 January 03.

Published in final edited form as:

J Comp Neurol. 2016 July 01; 524(10): 1999–2017. doi:10.1002/cne.23929.

Organization of the Sleep-Related Neural Systems in the Brain of the Harbour Porpoise (*Phocoena phocoena*)

Leigh-Anne Dell[1], **Nina Patzke**[1], **Muhammad A. Spocter**[1,2], **Jerome M. Siegel**[3], **Paul R. Manger**[1,*]

[1]School of Anatomical Sciences, Faculty of Health Sciences, University of the Witwatersrand, Parktown 2193, Johannesburg, Republic of South Africa

[2]Department of Anatomy, Des Moines University, Des Moines, Iowa 50312

[3]Department of Psychiatry, University of California, Los Angeles, Neurobiology Research 151A3, Veterans Administration Sepulveda Ambulatory Care Center, North Hills, California 91343

Abstract

The present study provides the first systematic immunohistochemical neuroanatomical investigation of the systems involved in the control and regulation of sleep in an odontocete cetacean, the harbor porpoise (*Phocoena phocoena*). The odontocete cetaceans show an unusual form of mammalian sleep, with unihemispheric slow waves, suppressed REM sleep, and continuous bodily movement. All the neural elements involved in sleep regulation and control found in bihemispheric sleeping mammals were present in the harbor porpoise, with no specific nuclei being absent, and no novel nuclei being present. This qualitative similarity of nuclear organization relates to the cholinergic, noradrenergic, serotonergic, and orexinergic systems and is extended to the γ-aminobutyric acid (GABA)ergic elements involved with these nuclei. Quantitative analysis of the cholinergic and noradrenergic nuclei of the pontine region revealed that in comparison with other mammals, the numbers of pontine cholinergic (126,776) and noradrenergic (122,878) neurons are markedly higher than in other large-brained bihemispheric sleeping mammals. The diminutive telencephalic commissures (anterior commissure, corpus callosum, and hippocampal commissure) along with an enlarged posterior commissure and supernumerary pontine cholinergic and noradrenergic neurons indicate that the control of unihemispheric slow-wave sleep is likely to be a function of interpontine competition, facilitated through the posterior commissure, in response to unilateral telencephalic input related to the drive for sleep. In addition, an expanded peripheral division of the dorsal raphe nuclear complex appears likely to play a role in the suppression of REM sleep in odontocete cetaceans. Thus, the

*CORRESPONDENCE TO: Paul Manger, School of Anatomical Sciences, Faculty of Health Sciences, University of the Witwatersrand, 7 York Road, Parktown, 2193, Johannesburg, Republic of South Africa. Paul.Manger@wits.ac.za.

ROLE OF AUTHORS

All authors had full access to all of the data in the study and take responsibility for the integrity of the data and the accuracy of the data analysis. LAD, NP, MAS, JMS, and PRM conceptualized the study. PRM obtained the brains, and LAD, NP, and PRM did the immunohistochemical staining and reconstructions. LAD and MAS undertook the quantitative and statistical analysis of the data. LAD and PRM wrote the manuscript, and the remaining authors contributed to the editing and improvement of the early drafts of the manuscript.

CONFLICT OF INTEREST STATEMENT

The authors declare no conflicts of interest.

current study provides several clues to the understanding of the neural control of the unusual sleep phenomenology present in odontocete cetaceans.

INDEXING TERMS:

Cetacea; Odontocete; Cetartiodactyla; mammalian sleep; unihemispheric sleep; brain evolution; RRID AB_2079751; RRID AB_10000323; RRID AB_10000343; RRID AB_10000340; RRID AB_10000321

The harbor porpoise *(Phocoena phocoena)* is a small, robust-bodied odontocete cetacean, weighing 50–80 kg (Price et al., 2005; Walløe et al., 2010), with a brain mass of approximately 500 g (Dell et al., 2012). They tend to inhabit the pelagic zone of northern temperate and subarctic waters and consume a diet of pelagic and semi-pelagic fish such as herring, whiting, and mackerel that provide a diet high in protein and fats (Rae, 1965; Gaskin, 1982; McLellan et al., 2002; Santos and Pierce, 2003). Odontocete cetaceans present with a unique physiology that allows for unihemispheric slow-wave sleep (USWS), in which the brain hemispheres alternate between periods of slow-wave sleep and wakefulness, plus the animals show little, if any, REM sleep and are moving continuously (Lyamin et al., 2008). To date, studies examining USWS have been mainly based on behavioral observations and electro-physiological studies (Serafetinides et al., 1972; Mukhametov et al, 1977; Supin and Mukhametov, 1986; Sobel et al., 1994; Oleksenko et al., 1996; Lyamin et al., 2008). Data relevant to the neuroanatomical structure of the neural systems associated with sleep are limited to the locus coeruleus complex of the bottlenose dolphin, the commissural systems in cetaceans, and the orexinergic system of the harbor porpoise (Manger et al., 2003; Lyamin et al., 2008; Dell et al., 2012). Although the locus coeruleus complex does not appear to differ significantly from land mammals, there is an enlarged posterior commissure (Lyamin et al., 2008) and reduced corpus callosum (Manger et al., 2010) in Odontocete cetaceans, and there are a significantly higher number of orexinergic neurons in the harbor porpoise compared with the giraffe, which has a similar brain mass (Dell et al., 2012). It is thus of interest to systematically examine the remaining neural systems associated with sleep and wakefulness in cetaceans to determine whether any other unusual and/or unique specializations have evolved that may contribute to the unique sleep phenomenology observed in Odontocete cetaceans.

The systems associated with the sleep and wake states are comprised of neurons that produce various neurotransmitters. These neurons depolarize in specific patterns during wake, slow-wave sleep, or REM sleep (Datta and MacLean, 2007; Lyamin et al., 2008; Takahashi et al., 2010; Dell et al., 2012; Bhagwandin et al., 2013; Petrovic et al., 2013). In relation to cetacean sleep, these neuronal systems have been extensively reviewed in Lyamin et al. (2008), but briefly, the γ-aminobutyric acid (GABA)ergic neurons of the basal forebrain are potent sleep promoters, whereas the cholinergic neurons of the basal forebrain are part of the arousal system. The hypothalamic orexinergic and histaminergic neurons are associated with arousal, whereas the midbrain/pontine cholinergic neurons are associated with wake and REM sleep. The GABAergic neurons of the midbrain/pons inhibit the activity of the serotonergic and noradrenergic neurons in this region, with the noradrenergic and

serotonergic neurons being active during wake and SWS, but inactive during REM, and the serotonergic neurons being implicated in inhibiting REM. Due to the relationship of these neuronal groups to the sleep–wake cycle, the present study examined the organization of the cholinergic, putative catecholaminergic, and serotonergic systems in the harbor porpoise. In addition, the distribution of the putative GABAergic neurons and terminal networks associated with the nuclei controlling and regulating sleep and wake was examined by staining for parvalbumin (PV), calbindin (CB), and calretinin (CR). Thus, we investigated the basal forebrain, diencephalon, and pons of the harbor porpoise. Stereological analysis of neuronal numbers was undertaken for the laterodorsal tegmental nucleus (LDT) and the pedunculopontine tegmental nucleus (PPT), as well as the locus coeruleus complex (LC). The aim of this study was to provide a clearer understanding of the neural basis of cetacean sleep regulation and control as well as better insight into the function and evolution of cetacean sleep phenomenology.

MATERIALS AND METHODS

Specimens

Brains from two adult male harbor porpoises *(Phocoena phocoena*) (body mass 49 kg and brain mass of 503 g; body mass 55 kg and brain mass of 486 g) were used in the current study. The animals were treated and used according to the guidelines of the University of Witwatersrand Animal Ethics Committee, which correspond with those of the National Institutes of Health for care and use of animals in scientific experimentation, and permission to collect the specimens was provided by the Greenland Institute for Natural Resources. Both harbor porpoises were obtained after being killed according to Greenlandic cultural practices and perfused via the heart with an initial rinse of 20 liters of 0.9% saline solution at a temperature of 4°C followed by 20 liters of 4% paraformaldehyde in 0.1 M phosphate buffer (PB). The brains were removed from the skull and postfixed in 4% paraformaldehyde in 0.1 M PB (24 hours at 4°C) and allowed to equilibrate in 30% sucrose in 0.1 M PB before being stored in an antifreeze solution (Manger et al., 2009).

Tissue selection and immunostaining

The basal forebrain, diencephalon, midbrain, and pons were dissected from the remainder of the brain, allowed to equilibrate in 30% sucrose in 0.1 M PB, and then frozen in crushed dry ice. The tissue block was mounted onto an aluminum stage, and coronal sections of 50 μm thickness were made using a sliding micro-tome. A 1:9 series was stained for Nissl, myelin, choline acetyltransferase (ChAT), tyrosine hydroxylase (TH), orexin (reported on previously by Dell et al., 2012), serotonin (5-HT), PV, CB, and CR. Nissl sections were mounted on 0.5% gelatine-coated glass slides and then cleared in a solution of 1:1 chloroform and 100% alcohol overnight, after which the sections were stained with 1% cresyl violet. The myelin series sections were refrigerated for 2 weeks in 5% formalin, mounted on 1.0% gelatin-coated slides, and stained with a modified silver stain (Gallyas, 1979).

The sections used for immunohistochemistry were initially treated for 30 minutes with an endogenous peroxidase inhibitor (49.2% methanol: 49.2% 0.1 M PB: 1.6% of 30% H_2O_2), followed by three 10-minute rinses in 0.1 M PB. The sections were then preincubated at

room temperature for 2 hours in a blocking buffer solution containing 3% normal serum (normal rabbit serum [NRS; Chemicon, Temecula, CA] for ChAT sections, and normal goat serum [NGS; Chemicon] for the remaining sections), 2% bovine serum albumin (BSA; Sigma, St. Louis, MO), and 0.25% Triton X-100 (Merck, Kenilworth, NJ) in 0.1 M PB. The sections were then placed in a primary antibody solution (blocking buffer with correctly diluted primary antibody) and incubated at 4°C for 48 hours under gentle shaking.

To reveal cholinergic neurons, anti-ChAT (AB144P, Chemicon, raised in goat) at a dilution of 1:2,500 was used. To reveal putative catecholaminergic neurons, anti-TH (AB151, Chemicon, raised in rabbit) was used at a dilution of 1:7,500. To reveal serotonergic neurons, anti-5-HT (AB938, Chemicon, raised in rabbit) at a dilution of 1:7,500 was used. To reveal CB-, CR-, and PV-containing neurons and terminal networks, we used anti-CB (CB38a, Swant, Bellinzona, Switzerland, raised in rabbit), anti-CR (7699/3H, Swant, raised in rabbit), and anti-PV (PV28, Swant, raised in rabbit), all at a dilution of 1:10,000. This was followed by three 10-minute rinses in 0.1 M PB, after which the sections were incubated in a secondary antibody solution for 2 hours at room temperature. The secondary antibody solution contained a 1:1 000 dilution of biotinylated anti-goat IgG (BA-5000, Vector, Burlingame, CA, for ChAT sections) or biotinylated anti-rabbit IgG (BA-1000, Vector, for the remaining sections) in a solution containing 3% NGS/NRS and 2% BSA in 0.1 M PB. This was followed by three 10-minute rinses in 0.1 M PB, after which the sections were incubated in AB solution (Vector) for 1 hour. After three further 10-minute rinses in 0.1 M PB, the sections were placed in a solution of 0.05% diaminobenzidine in 0.1 M PB for 5 minutes (2 ml/section), followed by the addition of 3 μl of 30% H_2O_2 to each 1 ml of solution in which each section was immersed.

Chromatic precipitation of the sections was monitored visually under a low-power stereomicroscope. This process was allowed to continue until the background staining of the sections was appropriate enough to assist with architectonic reconstruction without obscuring any immunopositive neurons. The precipitation process was stopped by immersing the sections in 0.1 M PB and then rinsing them twice more in 0.1 M PB. To check for nonspecific staining from the immunohistochemistry protocol, we omitted the primary antibody and the secondary antibody in selected sections, which produced no evident staining.

The immunohistochemically stained sections were mounted on 0.5% gelatin-coated slides and left to dry overnight. The sections were then dehydrated in graded series of alcohols, cleared in xylene, and coverslipped with Depex. The sections were viewed with a low-power stereomicroscope, and the architectonic borders of the sections were traced according to the Nissl- and myelin-stained sections by using a camera lucida. The immunostained sections were then matched to the drawings, and the immunopositive neurons were marked for ChAT, TH, and 5-HT. The immunopositive PV, CB, and CR neurons and the distribution of their terminal networks, due to their often very high number and density, were matched to these drawings under the microscope. Then the relative densities of immunopositive neurons and terminal networks were noted and photographed using higher powered light microscopy. The drawings were then scanned and redrawn using the Canvas 8 (Deneba) drawing program.

Antibody characterization and specificity

The antibodies used and associated details are listed in Table 1.

Choline acetyltransferase

To reveal neurons that produce acetylcholine as a neurotransmitter, we used the AB144P anti-ChAT goat polyclonal antibody from Merck-Millipore (AB144P, Merck-Millipore, Darmstadt, Germany; RRID AB_2079751) at a dilution of 1:2,500. This antibody reliably identifies cholinergic neurons in all regions of the brain across a range of vertebrate species (Kaiser et al., 2011; Laux et al., 2012). The pattern of staining found in the harbor porpoise was similar to that seen in a range of other mammals (Dell et al., 2010).

Tyrosine hydroxylase

To reveal the catecholaminergic neurons, which produce dopamine, noradrenaline, or adrenalin, we used the AB151 anti-TH rabbit polyclonal antibody from Merck-Millipore (AB151; RRID AB_10000323) at a dilution of 1:7,500. As TH is the rate-limiting enzyme in the production of catecholamines, this antibody reliably identifies catecholaminergic neurons across a broad range of vertebrate species (Piskuric et al., 2011). The pattern of staining found in the harbor porpoise was similar to that seen in a range of other mammals (Dell et al., 2010).

Serotonin

To reveal neurons that produce 5-HT as a neurotransmitter, we used the AB938 anti-5-HT rabbit polyclonal antibody from Merck-Millipore (AB938; no RRID number available) at a dilution of 1:7,500. The pattern of staining of serotonergic neurons in the midbrain and pons found in the harbor porpoise was similar to that seen in a range of other mammals (Dell et al., 2010).

Parvalbumin

To reveal neurons containing the calcium-binding protein PV, we used the PV28 anti-PV rabbit polyclonal antibody from Swant (PV28, Swant; RRID AB_10000343) at a dilution of 1:10,000. The pattern of staining within the neurons of the basal forebrain, diencephalon, and pons of the harbor porpoise was similar to that seen in other mammals (Gritti et al., 2003; Hirano et al., 2011; Bhagwandin et al., 2013).

Calbindin

To reveal neurons containing the calcium-binding protein CB, we used the CB38a anti-CB rabbit polyclonal antibody from Swant (CB38a; RRID AB_10000340) at a dilution of 1:10,000. The pattern of staining within the neurons of the basal forebrain, diencephalon, and pons of the harbor porpoise was similar to that seen in other mammals (Gritti et al., 2003; Bunce et al., 2013; Bhagwandin et al., 2013).

Calretinin

To reveal neurons containing the calcium-binding protein CR, we used the 7699/3H anti-CR rabbit polyclonal antibody from Swant (7699/3H; RRID AB_10000321) at a dilution of

1:10,000. The pattern of staining within the neurons of the basal forebrain, diencephalon, and pons of the harbor porpoise was similar to that seen in other mammals (Gritti et al., 2003; Adrio et al., 2011; Bhagwandin et al., 2013).

Stereological analysis

The numbers of cholinergic (ChAT)-immunopositive neurons in the LDT and PPT as well as the number of noradrenergic (TH)-immunopositive neurons in the LC were determined with stereological techniques. An Olympus BX-60 light microscope equipped with a three-axis motorized stage, video camera, and integrated Stereo-Investigator software (MicroBrightField, Colchester, VT, Version 8.0) was used for the stereological counts. Independent pilot studies for LDT, PPT, and LC were conducted on individual brain slices to optimize sampling parameters for cell counting (Table 2). Counting frames and grid sizes were optimized to achieve a mean coefficient of error of 10% or less (Gunderson and Jensen, 1987), and a guard zone of 5 μm was employed to avoid the introduction of errors due to sectioning artifacts (West et al., 1991). Section thickness was measured at every 5th sampling site, and the numbers of immunopositive neurons were counted in accordance with the principles of the optical fractionator method (West et al., 1991). In the PPT and LC, a standardized stereological approach using simple random sampling was implemented with counting frames of 200 μm × 200 μm and 150 μm × 150 μm, respectively. Corresponding grid sizes of 800 μm × 800 μm and 700 μm × 700 μm were used for the PPT and LC, respectively. Due to the relatively small size of the LDT nucleus, we used a modified unbiased stereological approach by performing exhaustive total counts using a counting frame and grid size of 200 μm × 200 μm. The optical fractionator method was used to computationally determine the number of ChAT+ cells in the LDT and PPT as well as the number of TH+ cells in the LC using the following formula:

$$N = Q/(\mathrm{SSF} \times \mathrm{ASF} \times \mathrm{TSF})$$

where N is the total estimated neuronal number, Q is the number of neurons counted, SSF is the section sampling fraction, ASF is the area subfraction (i.e., the ratio of the size of the counting frame to the size of the sampling grid), and TSF is the thickness subfraction (i.e., the ratio of the dissector height relative to cut section thickness). To determine the TSF, we used the average mounted section thickness calculated for each individual, subtracted the total vertical guard zones (10 μm) to give dissector height, and used the ratio of dissector height to cut section thickness (50 μm) to provide the TSF for each individual. The nucleator probe was used to estimate the mean volume and cross-sectional area of the immunopositive neurons, using five rays, and was used in conjunction with fractionator sampling (Gundersen, 1988).

RESULTS

The harbor porpoises studied exhibited a range of nuclei known to be involved in the regulation of the sleep–wake cycle, and these were, for the most part, similar to that previously observed in other mammals (Maseko et al., 2007; Dell et al., 2010, 2012; Bhagwandin et al., 2013). No differences in the nuclear organization of these systems,

or in the GABAergic neurons and terminal networks associated with these systems, were observed between the two individual animals studied; thus the description provided below applies to both animals, but where differences were found, these have been highlighted.

Cholinergic nuclei of the basal forebrain and pons

The cholinergic nuclei of the basal forebrain associated with the regulation of the sleep–wake cycle identified in the harbor porpoises included the diagonal band of Broca, the islands of Calleja and olfactory tubercle, and the nucleus basalis. Within the pons, we identified the PPT and the LDT. The diagonal band of Broca was located in the ventromedial aspect of the cerebrum, anterior and slightly ventral to the anterior pole of the hypothalamus and medial to the nucleus accumbens (Figs. 1A–D, 2A). It contained a moderate density of bipolar neurons, which were observed to be fusiform in shape. The dendrites of these neurons were arranged in a vertical orientation, parallel to the medial wall of the cerebral hemisphere (Fig. 2A). The cholinergic neurons forming the islands of Calleja and olfactory tubercle were identified in the floor of the cerebrum, lateral to the diagonal band (Fig. 1A–D). A high density of cholinergic neurons was observed within these nuclei, but no specific somal or dendritic orientation of these neurons was observed. The cholinergic neurons within the islands of Calleja and olfactory tubercle exhibited a variety of morphologies, including round unipolar neurons, spherical or oval bipolar neurons, and triangular multipolar neurons. The clusters forming the islands of Calleja were not as distinct as observed in other mammals (Calvey et al., 2013), perhaps due to the lack of the olfactory system in the Odontocete cetaceans. The cholinergic neurons forming the nucleus basalis were identified caudal to the globus pallidus and dorsomedial to the olfactory tubercle (Fig. 1B–D). The nucleus basalis contained a high density of oval bipolar neurons and multipolar neurons with similar somal areas, and both types had dendrites orientated in a lateroventral plane.

A moderate density of cholinergic neurons, forming the PPT nucleus, was found throughout the parvocellular region of the pontine tegmentum (Fig. 1H–M). These neurons began at the level of the oculomotor nucleus and extended caudally to the level of the trigeminal motor nucleus. Stereological analysis revealed that there were approximately 111,134 ChAT+ neurons in the PPT. These neurons had a mean somal volume of 2,648.00 μm^3 (± 1,395.15 SD) and a mean surface area of 1,196.26 μm^2 (± 568.27 SD), and were mostly multipolar (Fig. 3A, Table 3). The cholinergic neurons forming the LDT nucleus were localized within the lateroventral periventricular gray matter of the pons (Fig. 1I–L). A low density of multipolar cholinergic neurons, exhibiting no specific dendritic orientation, was observed within this nucleus (Fig. 3A). Stereological analysis revealed that there were approximately 15,642 cholinergic neurons forming this nucleus, and these neurons had a mean somal volume of 2,790.14 μm^3 (± 1,590.38 SD) and a mean surface area of 1,136.20 μm^2 (± 537.93 SD), being very similar in size to those found in the PPT (Table 3).

Catecholaminergic nuclei of the locus coeruleus complex

The locus coeruleus complex, found within the pons, could be divided into five distinct divisions including the subcoeruleus diffuse (A7d), subcoeruleus compact (A7sc), locus coeruleus diffuse (A6d), fifth arcuate nucleus (A5), and dorsomedial (A4) divisions (Fig.

1I–P). The A7d was located within the parvocellular portion of the pontine tegmentum, extending from the periventricular gray matter, laterally to the edge of the pontine tegementum, encircling the ventral aspect of the superior cerebellar peduncle. In its most caudal aspect, a few neurons belonging to the A7d could be observed in the ventral white matter of the cerebellum (Fig. 1P). A moderate density of multipolar TH-immunoreactive neurons, showing no specific dendritic orientation, could be observed throughout the A7d, although the density of these neurons became less toward the lateral and ventral edges of the nucleus. In the dorsal aspect of the pontine tegmentum, immediately adjacent to the ventrolateral aspect of the pontine periventricular gray matter, a high density of TH-immunoreactive multipolar neurons, showing no specific dendritic orientation, formed the A7sc division of the locus coeruleus (Fig. 4A). The A7sc and the A7d formed a continuous nucleus, only being distinguished by the density of neurons forming these two divisions.

The A6d division of the locus coeruleus complex was identified in the ventrolateral aspect of the pontine periventricular gray matter (Fig. 1J–M), showing some overlap with the caudal pole of the LDT nucleus. The A6d nucleus contained a low density of TH-immunopositive neurons that showed no specific dendritic orientation (Fig. 4A). A small number of TH-immunoreactive neurons ventral to the trigeminal motor nucleus and medial to the descending limb of the facial nerve formed the fifth arcuate nucleus (A5) (Fig. 1O), whereas a small cluster of TH-immunoreactive neurons in the dorsolateral aspect of the periventricular gray matter, medial to the dorsal aspect of the superior cerebellar peduncle formed the dorsomedial division of the locus coeruleus complex (Fig. 1N). Stereological analysis revealed that the entire locus coeruleus complex contained approximately 122,878 neurons that had a mean somal volume of 1,624.16 μm^3 (± 816.66 SD) and an average surface area of 647.99 μm^2 (± 219.39 SD) (Table 3). Thus, the neurons forming the locus coeruleus complex were markedly smaller in size than the cholinergic neurons of the PPT and LDT nuclei, although the total numbers of neurons were similar (LC = 122,878; PPT + LDT = 126,776).

Serotonergic nuclei of the dorsal raphe complex

The neurons forming the dorsal raphe complex, revealed with immunohistochemistry to 5-HT, were located mostly near the midline within the periaqueductal and periventricular gray matter, with some neurons extending into the dorsal midbrain/pontine tegmentum. Within the dorsal raphe nuclear complex, six distinct nuclei, extending from the level of the oculomotor nucleus to the trigeminal motor nucleus (Fig. 1H–N), were identified. These six nuclei were the dorsal raphe interfasicular (DRif), dorsal raphe ventral (DRv), dorsal raphe dorsal (DRd), dorsal raphe lateral (DRl), dorsal raphe peripheral (DRp), and dorsal raphe caudal (DRc) nuclei.

The DRif nucleus was located between the two medial longitudinal fasciculi in the ventralmost aspect of the periaqueductal gray matter and contained a high density of spherical or oval-shaped bipolar neurons that exhibited a dorsoventral dendritic orientation. This nucleus was continuous ventrally with the serotonergic neurons forming the median raphe nucleus (MnR).

The DRv nucleus was identified in the ventromedial region of the periaqueductal gray matter, immediately dorsal to the DRif. The DRv contained a moderate density of multipolar serotonergic neurons that were spherical in shape, but no specific dendritic orientation was noted.

The DRd was located dorsal to the DRv within the periaqueductal gray matter. The morphology and lack of dendritic orientation of the DRd neurons resembled that seen in the DRv, but the DRd contained a somewhat higher density of serotonergic neurons.

The DRl nucleus was found dorsolateral to both the DRd and DRv within the periaqueductal gray matter (Fig. 5A). The serotonergic neurons of the DRl exhibited a low to moderate density and were mostly multipolar neurons showing no specific dendritic orientation. The soma of the neurons forming the DRl were larger than those observed in the DRif, DRv, and DRd, but were similar in size and shape to those forming the DRp nucleus (Fig. 5A).

The DRp nucleus was identified in the ventrolateral portion of the periaqueductal gray matter and exhibited neurons that infused the adjacent midbrain tegmental region, being the only nucleus of the dorsal raphe to contain neurons outside of the central gray matter. The DRp contained a very high density of multipolar serotonergic neurons, all displaying no specific dendritic orientation (Fig. 5A). In the case of the harbor porpoise, the DRp seems to be expanded and have a greater number of neurons than seen in other mammals. The DRc nucleus was identified within the most caudal region of the periventricular gray matter (Fig. 1L–M). This nucleus contained a low density of serotonergic neurons that exhibited a similar morphology to the neurons observed in the DRl and DRp. This nucleus likely represents a caudal amalgamation of the neurons of the DRl and DRp.

Neurons and terminal networks containing calcium binding proteins

Immunohistochemistry for the calcium binding proteins CB, CR, and PV was performed to label subtypes of GABAergic neurons that are active during different sleep–wake states and during transitions between these states (Siegel, 2004; Jones, 2007; Bhagwandin et al., 2013). The results described below, summarized in Table 4, detail the density of neurons and terminal networks immunopositive for CB, CR, and PV in relation to the sleep–wake-related nuclei associated with the cholinergic, catecholaminergic, serotonergic, and orexinergic systems as well as the thalamic reticular nucleus.

Neurons and terminal networks containing calcium binding proteins in the basal forebrain and pontine cholinergic system

A low density of CB-immunopositive neurons was identified in the diagonal band of Broca and nucleus basalis with a low-density CB-immunopositive terminal network being identified in the diagonal band of Broca, whereas no CB-immunopositive terminal network was observed in the nucleus basalis (Fig. 2). A high density of CB-immunopositive neurons was located in the islands of Calleja and the olfactory tubercle, but the CB-immunopositive terminal network density was low in this region. A moderate density of CR-immunopositive neurons was found in both the diagonal band of Broca and the islands of Calleja and olfactory tubercle, with the former exhibiting a moderately dense CR-immunopositive terminal network and the latter displaying a low-density CR-immunopositive terminal

network (Fig. 2). The Nucleus basalis contained a moderate density of CR-immunopositive neurons, but a low-density CR-immunopositive terminal network. A low density of PV-immunopositive neurons was observed in the diagonal band of Broca and the islands of Calleja and olfactory tubercle, with a low-density PV-immunopositive terminal network in the diagonal band of Broca, whereas the islands of Calleja and olfactory tubercle contained no PV-immunopositive terminal network (Fig. 2). Although the nucleus basalis had a moderate density of PV-immunopositive neurons, no PV-immunopositive terminal network was observed. A high density of CB-immunopositive neurons and terminal networks was observed in the LDT (Fig. 3). A moderate density of CB-immunopositive neurons was seen in the PPT, but a high density CB-immunopositive terminal network was present (Fig. 3). A moderate density of CR-immunopositive neurons and a low-density CR-immunopositive terminal network was observed in both the LDT and PPT (Fig. 3). No PV-immunopositive neurons were found in the LDT and PPT, but a low-density PV-immunopositive terminal network was observed in both nuclei (Fig. 3).

Neurons and terminal networks containing calcium binding proteins in the locus coeruleus complex

A high density of CB-immunopositive neurons and a high-density CB-immunopositive terminal network was identified in the A7sc (Fig. 4). The A7d and A6d both exhibited moderate densities of CB-immunopositive neurons and moderately dense CB-immunopositive terminal networks (Fig. 4). A low density of CR-immunopositive neurons coupled with a moderately dense CR-immunopositive terminal network was observed in both the A7sc and A7d (Fig. 4). A moderate density of CR-immunopositive neurons and a moderately dense CR-immunopositive terminal network was identified in the A6d (Fig. 4). A low density of PV-immunopositive neurons and a low-density PV-immuno-positive terminal network was observed in all three nuclei (Fig. 4).

Neurons and terminal networks containing calcium binding proteins in the dorsal raphe complex

A low density of CB-immunopositive neurons with a low-density CB-immunopositive terminal network was found in the DRif. A moderate density of CB-immunopositive neurons was observed in the DRv, DRd, DRl, and DRc, and this was coupled with a low, moderate, high, and moderate density of CB-immunopositive terminal networks, respectively (Fig. 5). A moderate density of CB-immunopositive neurons and a moderately dense CB-immunopositive terminal network was seen in the DRp (Fig. 5). Neither CR-immunopositive neurons nor terminal networks were found in the DRif. The DRv and DRc both had a low density of CR-immunopositive neurons coupled with moderately dense CR-immunopositive terminal networks (Fig. 5). A moderate density of CR-immunopositive neurons and a moderately dense CR-immunopositive terminal network was seen in the DRd, whereas a high density of CR-immunopositive neurons and high-density CR-immuno-positive terminal networks were observed in both the DRl and DRp (Fig. 5). Neither PV-immunopositive neurons nor terminal networks were identified in the DRif. A low density of PV-immunopositive neurons and low-density PV-immunopositive terminal networks were seen in the DRv, DRd, DRl, and DRp (Fig. 5). No PV-immunopositive neurons were found

in the DRc, but a moderately dense PV-immunopositive terminal network was seen in this nucleus.

Neurons and terminal networks containing calcium binding proteins in the hypothalamic orexinergic complex

The distribution of the orexinergic neurons in the hypothalamus of the harbor porpoise has been reported previously (Dell et al., 2012). A moderate density of CB-immunopositive neurons and a moderately dense CB terminal network was observed in both the main magnocellular cluster and the medial parvocellular cluster. A low density of CB-immunopositive neurons was identified in the optic tract cluster, but this region displayed a moderately dense CB-immunopositive terminal network. The zona incerta cluster had a moderate density of CB-immunopositive neurons coupled with a low-density CB-immunopositive terminal network. A moderate density of CR-immunopositive neurons coupled with a low-density CR-immunopositive terminal network was observed in both the main magnocellular cluster and the medial parvocellular cluster. The optic tract and zona incerta clusters both exhibited low densities of CR-immunopositive neurons with no distinct terminal networks present. A low density of PV-immunopositive neurons was located in the main magnocellular cluster, but PV-immunopositive neurons were not observed in the other orexinergic clusters. All regions where orexinergic neurons were found evinced no PV-immunopositive terminal networks.

Neurons and terminal networks containing calcium binding proteins in thalamic reticular nucleus

The thalamic reticular nucleus of the harbor porpoise occupied a position typical of mammals (Fig. 6). Within this nucleus, no CB-immunopositive neurons and a very low-density CB-immunopositive terminal network was observed. A high density of CR-immunopositive neurons coupled with a moderately dense CR-immunopositive terminal network was identified in the thalamic reticular nucleus. A high density of PV-immunopositive neurons and a high-density PV-immunopositive terminal network was observed within the thalamic reticular nucleus. Interestingly, the CR-immunopositive neurons were markedly larger, with more dendrites emanating from the cell body than the PV-immunopositive neurons (Fig. 6).

DISCUSSION

This study examined the neural systems in the harbor porpoise brain that are likely to be related to the control and regulation of sleep and wake to determine if there are qualitative or quantitative differences in these neural systems that may explain the physiological and behavioral aspects of cetacean-type sleep (Lyamin et al., 2008). The nuclear organization of the cholinergic, catecholaminergic, and serotonergic systems, from the basal forebrain through to the pons, was very similar to that seen in many other mammals (Manger et al., 2003; Bhagwandin et al., 2008; Kruger et al., 2010; Dell et al., 2010, 2012, 2013; Calvey et al., 2013). The expression of the calcium binding proteins (PV, CB, and CR, mostly occurring in GABAergic neurons, but see Gritti et al., 2003) in neurons and terminal networks associated with these nuclei, which are active/inactive during different phases

of the sleep–wake cycle, showed a similar organization to that seen in other mammals (Bhagwandin et al., 2013), although minor differences were noted. As cetaceans undergo USWS with minimal REM sleep (Mukhametov, 1987; Lyamin et al., 2008), a feature not seen in terrestrial mammals studied to date (Tobler, 1995), one would anticipate that their neural circuitry may show distinct differences from that of terrestrial mammals, but the present study demonstrates that this is not the case. Thus, there must be other explanations or differences not detected with the current methodology that may better explain cetacean sleep phenomenology.

Similarities in the nuclear organization of the sleep neural systems across mammals

The neural systems associated with the regulation and control of sleep and wake examined in this study of the harbor porpoise, the cholinergic nuclei of the basal forebrain and pons, the locus coeruleus complex, and the dorsal raphe complex, showed no unique nuclei or nuclear subdivisions compared with terrestrial mammals previously studied or compared with the locus coeruleus complex of the bottlenose dolphin (Manger et al., 2003; Dell et al., 2010, 2012; Calvey et al., 2013). Thus, it can be concluded that, at the analytical level of nuclear organization, the neural systems associated with sleep and wake in mammals are strongly conserved across species. It would seem likely that these nuclei execute similar functions in relation to global neural modulation in both terrestrial and aquatic mammals despite the differences in sleep physiology of the aquatic mammals (Lyamin et al., 2008). These findings support the conclusions of Tobler (1995), which indicated that although sleep is functionally different across mammals, the mechanisms by which sleep is regulated have a fundamental cohesiveness.

The basal forebrain cholinergic nuclei, which receive strong input from the diencephalon and brainstem (Petrovic et al., 2013), are primarily responsible for changing cortical activity from a slow deactivated phase (slow-wave sleep) to an active high-frequency phase (wake/REM) (Dringenberg and Olmstead, 2003), a process that occurs independently between the two cerebral hemispheres in cetaceans (Mukhametov, 1987; Lyamin et al., 2008). Although numerous studies have identified the significance of the pontine cholinergic nuclei (LDT and PPT) in REM sleep (Lu et al., 2006), it is unclear whether true REM sleep occurs in cetaceans (Lyamin et al., 2008). Even so, the harbor porpoise exhibited no noticeable anatomical differences of the LDT and PPT compared with the terrestrial mammals studied to date (Dell et al., 2010, 2012; Calvey et al., 2013). What is often less emphasized is the role of the LDT and PPT in arousal, motor control such as breathing, and organization of cortical activity during SWS (Lydic and Baghdoyan, 1993; Takakusaki et al., 2004; Datta and Maclean, 2007). Thus, in terms of the understanding of cetacean USWS, it would appear that these latter functions are pivotal for cetacean sleep phenomenology. The organization of the locus coeruleus complex in the harbor porpoise was similar to that of the bottlenose dolphin (Manger et al., 2003) and indeed to that of most mammals (Dell et al., 2010; Calvey et al., 2013). Thus, it is reasonable to postulate, based on the conserved anatomical organization, that the role of the locus coeruleus complex in cetacean USWS would be, as in other mammals, arousal and maintenance of muscle tone (Manger et al., 2003; Lyamin et al., 2008; Takahashi et al., 2010). The serotonergic dorsal raphe complex in cetaceans would also appear to execute functions similar to that observed in terrestrial

mammals by promoting wakefulness and inhibiting REM sleep (Monti, 2011); however, the drive to inhibit REM sleep may be greater in cetaceans, as the loss of muscle tone during REM sleep may result in drowning and hypothermia (Manger et al., 2003; Lyamin et al., 2008). The expansion of the peripheral division of the dorsal raphe nuclear complex of the harbor porpoise, one notable qualitative difference between cetaceans and other mammals, may thus facilitate the suppression of REM sleep in cetaceans.

Similarities of the GABAergic systems in sleep associated nuclei across mammals

GABAergic neurons have been identified throughout the basal forebrain, diencephalon, midbrain, and pons and are often, but not always, colocalized with calcium binding proteins (Gritti et al., 2003; Lyamin et al., 2008; Bhagwandin et al., 2013). Thus, the localization of the calcium binding proteins serves as a useful marker for GABAergic neurons (Celio, 1986; Jacobowitz and Winsky, 1991; Rogers, 1992; Silver et al., 1996) and divides them into three subtypes, although as this is not always the case, these results must be interpreted with caution (Gritti et al., 2003). The GABAergic neurons are primarily considered to be promoters of sleep, as physiological studies show that they fire maximally during SWS (Szymusiak, 1995; Szymusiak et al., 2001; Siegel, 2004). GABAergic neurons relating to the sleep and wake neural systems in cetaceans have not been studied previously (Lyamin et al., 2008). When the harbor porpoise is compared with other mammals, the presence of PV in neurons and terminal networks within the basal forebrain, pons, hypothalamus, and thalamic reticular nucleus is similar (Bhagwandin et al., 2013).

There was an overall decrease in the density of CB and CR terminal networks in the cholinergic basal forebrain and pontine nuclei in the harbor porpoise compared with previous mammalian studies (Bhagwandin et al., 2013). An overall decrease in the density of CB and CR neurons and terminal networks in relation to orexinergic nuclei was observed in the harbor porpoise, which could indicate that the orexinergic neurons do not contribute as significantly to arousal in the harbor porpoise, and thus fewer GABAergic neurons would be needed to inhibit arousal and allow for sleep (Gritti et al., 2003). There was an overall increase in the density of CB neurons and the density of CR terminal networks within the locus coeruleus complex compared with other mammals (Bhagwandin et al., 2013). This could be due to an overall increased occurrence of depolarization of the locus coeruleus neurons in cetaceans (Manger et al., 2003). In general, an overall decrease in the density of CB neurons and an increase in the density of CR neurons and terminal networks were observed in the sleep- and wake-associated nuclei in the brain of the harbor porpoise compared with previous studies (Bhagwandin et al., 2013), with CR being considered an important regulator of the sleep–wake cycle (Baker et al., 1991; Michelson et al., 2007). Despite these differences in the density of GABAergic neurons and terminal networks in the sleep-related nuclei of the harbor porpoise, there is striking similarity with other mammals, emphasizing conservation of the anatomical substrate governing the sleep–wake cycle across mammals, even though marked differences in sleep patterns may exist.

So how do odontocete cetaceans attain USWS and minimal REM sleep?

The neural systems associated with sleep in the harbor porpoise brain do not differ in a dramatic way from other mammals such that we can point to the presence or absence

of a particular nucleus, or the presence or absence of a GABAergic input to a particular nucleus, to explain the presence of USWS and minimal REM in odontocete cetaceans (Lyamin et al., 2008). As structure is inherently related to function, there must be an alternative explanation for how the neuroanatomy relates to the execution of the physiology of USWS in cetaceans, and perhaps a quantitative rather than a qualitative explanation may be more appropriate. During USWS in cetaceans, the cerebral hemispheres are clearly activated in different ways, with one hemisphere showing slow waves while the other exhibits a desynchronized electroencephalogram (EEG) associated with wake (Lyamin et al., 2008); thus physiological isolation of the hemispheres during sleep is clearly important. The three largest telencephalic hemispheres (the anterior commissure, corpus callosum, and hippocampal commissure)are all greatly reduced in size in cetaceans, presumably with lower axonal numbers, compared with other mammals (Wilson, 1933; Manger et al., 2010; Patzke et al., 2015). This quantitative change, but not a qualitative change as the commissures are still present, will provide anatomical assistance to the physiological hemispheric independence/incoherence during slow-wave sleep in cetaceans, but is likely not the generator of USWS. In contrast, the posterior commissure of cetaceans is greatly enlarged in comparison with other mammals (Lyamin et al., 2008). This quantitative increase in size indicates that the region of the brain involved in the generation of USWS is likely to be found caudal to this commissure, in the midbrain and pontine regions.

It has been shown that the harbor porpoise has a greater number of orexinergic neurons in the hypothalamus than the giraffe (an artiodactyl that has a similar brain mass), this being 21,254 neurons compared with 15,003 neurons (Dell et al., 2012), but that cetaceans have lower density orexinergic terminal networks in the cerebral cortex than artiodactyls (Dell et al., 2015). Humans have approximately 70,000 orexinergic neurons in the hypothalamus (Thannickal et al., 2000). In the current study it was shown that the cholinergic nuclei of the pons (LDT and PPT) have a combined neuron count of 126,776 neurons, whereas the locus coeruleus complex has a combined neuron count of 122,878 neurons. Stereological assessment of the numbers of neurons in these nuclei in the human brain (which is three times larger) has provided neuronal numbers of around 20,000 for the LDT/PPT and 22,000 for the locus coeruleus complex (Manaye et al., 1999; Mouton et al., 1994). Thus, again, we have several quantitative differences in the cetaceans compared with other mammal species of similar brain mass that have been studied—in this case, fewer orexinergic neurons than humans, but more than giraffes, and approximately six times more pontine cholinergic and noradrenergic neurons than humans. The increase in pontine cholinergic and noradrenergic neurons, along with the noted, but not quantified, increase in the serotonergic neurons of the peripheral division of the dorsal raphe, are in accord with the idea that the regions controlling the production of USWS and suppressing REM sleep in cetaceans are caudal to the posterior commissure. We are not suggesting that the brainstem produces the slow waves (as this is likely still a forebrain function, because the neural systems involved do not differ across mammalian species), rather, we are suggesting that the brainstem controls when one hemisphere is in slow-wave sleep while the other has a desynchronized EEG in the cetaceans.

Although clearly the larger numbers of cholinergic, noradrenergic, and serotonergic neurons in the midbrain and pons play a role in this physiology, how they achieve this is currently

unknown. Speculatively, we could propose that the supernumerary neurons in these regions, instead of all projecting forward to their standard ipsilateral forebrain targets (such as the dorsal thalamic relay, intralaminar and reticular nuclei, lateral hypothalamus, and basal forebrain; Saper et al., 2010), may either project to the contralateral forebrain targets or the contralateral pontine nuclear equivalent through the posterior commissure. This speculation is supported by the high number of TH axons found in the posterior commissure of the bottlenose dolphin (Lyamin et al., 2008). In this way, forebrain centers that drive the need for sleep maintain their standard projection to the ipsilateral pontine nuclei, which then through posterior commissural competition, based on the strength of the descending hemispheric signal, determine which hemisphere enters slow-wave sleep and which retains a desynchronized EEG. This idea is supported by the observation of unilateral sleep rebound following USWS deprivation in dolphins (Supin and Mukhametov, 1986). In this way, the same nuclear organization of the neural systems involved in sleep can generate either bilateral synchronization in the cerebral hemispheres, as seen in most mammals and cetaceans when awake, or unilateral incoherence, as seen in cetaceans when asleep, by enlarging what are likely to be pre-existing, but minor, connections in the brains of most mammals.

Thus, quantitative changes, in both neural numbers and the strength of connectivity, but not qualitative changes such as the addition or loss of nuclei or connections, may lead to both the hemispheric incoherence observed in cetacean USWS and the suppression of REM sleep. Further qualitative and quantitative studies of the neural systems involved in the control and regulation of sleep in the baleen whales (mysticetes) and the closely related artiodactyls, such as the river hippopotamus, need to be performed to confirm and extend the observations made in the present study and provide a clearer understanding of cetacean sleep phenomenology.

ACKNOWLEDGMENTS

We thank the Greenland Institute of Natural Resources for allowing us to obtain the specimens of harbor porpoise brains. In particular we thank Mads-Peter Heide-Jørgensen, Fernando Ugarte, Finn Christensen, and Knud Kreutzmann for all the assistance they afforded us with the acquisition of these specimens.

Grant sponsor: the South African National Research Foundation; Grant number: Innovation scholarship (to L.D.); Grant sponsor: Society, Ecosystems and Change, SeaChange; Grant number: KFD2008051700002 (to P.R.M.); Grant sponsor: ISN-CAEN travel grant (to L.D.); Grant sponsor: Postdoc-Programme of the German Academic Exchange Service (DAAD; fellowship to N.P.); Grant sponsor: Des Moines University; Grant number: IOER R&G and Startup grant 12-13-03 (to M.A.S.); Grant sponsor: National Institutes of Health; Grant number: DA 2R01MH064109 (to J.M.S.); Grant sponsor: Department of Veterans Affairs (to J.M.S).

Abbreviations

III	oculomotor nucleus
IV	trochlear nucleus
Vmot	motor trigeminal nucleus
Vsens	sensory trigeminal nucleus
VIIv	ventral division of facial nerve nucleus

3V	third ventricle
4V	fourth ventricle
5n	trigeminal nerve
7n	descending arm of facial nerve
A4	dorsal medial division of locus coeruleus
A5	fifth arcuate nucleus
A6d	diffuse portion of locus coeruleus
A7d	nucleus subcoeruleus, diffuse portion
A7sc	nucleus subcoeruleus, compact portion
A9pc	substantia nigra, pars compacta
A9l	substantia nigra, lateral
A9m	substantia nigra, medial
A9v	substantia nigra, ventral
A10	ventral tegmental area
A10c	ventral tegmental area, central
A10d	ventral tegmental area, dorsal
A10dc	ventral tegmental area, dorsal caudal
A11	caudal diencephalic group
A12	tuberal cell group
A14	rostral periventricular nucleus
A15d	anterior hypothalamic group, dorsal division
B9	supralemniscal serotonergic nucleus
Ca	cerebral aqueduct
Cb	cerebellum
Cic	commissure of the inferior colliculus
CLi	caudal linear nucleus
CO	cochlear nuclear complex
Diag.B	diagonal band of Broca
DRc	dorsal raphe nucleus, caudal division

DRd	dorsal raphe nucleus, dorsal division
DRif	dorsal raphe nucleus, interfascicular division
DRl	dorsal raphe nucleus, lateral division
DRp	dorsal raphe nucleus, peripheral division
DRv	dorsal raphe nucleus, ventral division
DT	dorsal thalamus
EW	Edinger–Westphal nucleus
fr	fasciculus retroflexus
GC	central grAy matter
GiCRt	gigantocellular reticular column
GP	globus pallidus
Hbm	medial habenular nucleus
Hyp	hypothalamus
Hyp.d	dorsal hypothalamic cholinergic nucleus
Hyp.l	lateral hypothalamic cholinergic nucleus
Hyp.v	ventral hypothalamic cholinergic nucleus
IC	inferior colliculus
Ic	internal capsule
IP	interpeduncular nucleus
Is.Call	islands of Calleja
LDT	laterodorsal tegmental nucleus
Lfp	longitudinal fasciculus of the pons
LVe	lateral vestibular nucleus
Mcp	middle cerebellar peduncle
mlf	medial longitudinal fasciculus
MnR	median raphe nucleus
N.Bas	nucleus basalis
N.Ell	nucleus ellipticus
NEO	neocortex

OC	optic chiasm
ON	optic nerve
OT	optic tract
P	putamen nucleus
PBg	parabigeminal nucleus
PC	cerebral peduncle
pc	posterior commissure
PCRt	parvocellular reticular column
pit. stalk	stalk of pituitary gland
pVII	superior salivatory nucleus
PPT	pedunculopontine tegmental nucleus
R	thalamic reticular nucleus
Rmc	red nucleus, magnocellular division
RMg	raphe magnus nucleus
RMR	rostral mesencephalic raphe cluster
RtTg	reticulotegmental nucleus
SC	superior colliculus
Scp	superior cerebellar peduncle
SON	superior olivary nucleus
Sp5	spinal trigeminal tract
TOL	olfactory tubercle
VCO	ventral cochlear nucleus
VPO	ventral pontine nucleus
xscp	decussation of the superior cerebellar peduncle
zi	zona incerta

LITERATURE CITED

Adrio F, Rodriguez-Moldes I, Anadon R. 2011. Distribution of glycine immunoreactivity in the brain of the Siberian sturgeon (*Acipenser baeri*): comparison with γ-aminobutyric acid. J Comp Neurol 519:1115–1142. [PubMed: 21344405]

Baker KG, Halliday GM, Hornung JP, Geffen LB, Cotton RG, Tork I. 1991. Distribution, morphology and number of monoamine synthesizing and substance P-containing neurons in the human dorsal raphe nucleus. Neuroscience 42:757–775. [PubMed: 1720227]

Bhagwandin A, Fuxe K, Bennett NC, Manger PR. 2008. Nuclear organization and morphology of cholinergic, putative catecholaminergic and serotonergic neurons in the brains of two species of African mole-rat. J Chem Neuroanat 35:371–387. [PubMed: 18407460]

Bhagwandin A, Gravett N, Bennett NC, Manger PR. 2013. Distribution of parvalbumin, calbindin and calretinin containing neurons and terminal networks in relation to sleep associated nuclei in the brain of the giant Zambian mole-rat (*Fukomys mechowii*). J Chem Neuroanat 52:69–79. [PubMed: 23796985]

Bunce JG, Zikopoulos B, Feinberg M, Barbas H. 2013. Parallel prefrontal pathways reach distinct excitatory and inhibitory systems in memory-related rhinal cortices. J Comp Neurol 521:4260–4283. [PubMed: 23839697]

Calvey T, Patzke N, Kaswera C, Gilissen E, Bennett NC, Manger PR. 2013. Nuclear organization of some immunohistochemically identifiable neural systems in three Afrotherian species—*Potomogale velox*, *Amblysomus hottentotus* and *Petrodromus tetradactylus*. J Chem Neuroanat 50–51:48–65.

Celio MR. 1986. Parvalbumin in most gamma-aminobutyric acid containing neurons of the rat cerebral cortex. Science 231:995–997. [PubMed: 3945815]

Datta S, MacLean RR. 2007. Neurobiological mechanisms for the regulation of mammalian sleep-wake behavior: reinterpretation of historical evidence and inclusion of contemporary cellular and molecular evidence. Neurosci Biobehav Rev 31:775–824. [PubMed: 17445891]

Dell LA, Kruger JL, Bhagwandin A, Jillani NE, Pettigrew JD, Manger PR. 2010. Nuclear organization of cholinergic, putative catecholaminergic and serotonergic systems in the brains of two megachiropteran species. J Chem Neuroanat 40:177–195. [PubMed: 20566331]

Dell LA, Patzke N, Bhagwandin A, Bux F, Fuxe K, Barber G, Siegel JM, Manger PR. 2012. Organization and number of orexinergic neurons in the hypothalamus of two species of Cetartiodactyla: a comparison of giraffe (*Giraffa came-lopardalis*) and harbour porpoise (*Phocoena phocoena*). J Chem Neuroanat 44:98–109. [PubMed: 22683547]

Dell LA, Kruger JL, Pettigrew JD, Manger PR. 2013. Cellular location and major terminal networks of the orexinergic system in the brain of two megachiropterans. J Chem Neuroanat 53:64–71. [PubMed: 24041616]

Dell LA, Spocter MA, Patzke N, Karlson KÆ, Alagaili AN, Bennett NC, Muhammed OB, Bertelsen MF, Siegel JM, Manger PR. 2015. Orexinergic bouton density is lower in the cerebral cortex of cetaceans compared to artiodactyls. J Chem Neuroanat 68:61–76. [PubMed: 26232521]

Dringenberg HC, Olmstead MC. 2003. Integrated contributions of the basal forebrain and thalamus to neocortical activation elicited by pedunculopontine tegmental stimulation in urethane-anesthetized rats. Neuroscience 119:839–853. [PubMed: 12809705]

Gallyas F 1979. Silver staining of myelin by means of physical development. Neurol Res 1:203–209. [PubMed: 95356]

Gaskin DE. 1982. The ecology of whales and dolphins. London: Heinemann Educational Books.

Gritti I, Manns ID, Mainville L, Jones BE. 2003. Parvalbumin, calbindin, or calretinin in cortically projecting and GABAergic, cholinergic, or glutaminergic basal forebrain neurons of the rat. J Comp Neurol 458:11–31. [PubMed: 12577320]

Gundersen HJ. 1988. The nucleator. J Microsc 151:3–21. [PubMed: 3193456]

Hirano AA, Brandstatter JH, Morgans CW, Brecha NC. 2011. SNAP25 expression in mammalian retinal horizontal cells. J Comp Neurol 519:972–988. [PubMed: 21280047]

Jacobowitz DM, Winsky L. 1991. Immunocytochemical localization of calretinin in the forebrain of the rat. J Comp Neurol 304:198–218. [PubMed: 2016417]

Jones EG. 2007. The thalamus. Cambridge, UK: Cambridge University Press.

Kaiser A, Alexandrova O, Grothe B. 2011. Urocortin-expressing olivocochlear neurons exhibit tonotopic and developmental changes in the auditory brainstem and in the innevation of the cochlea. J Comp Neurol 519:2758–2778. [PubMed: 21491428]

Kruger JL, Dell LA, Pettigrew JD, Manger PR. 2010. Cellular location and major terminal networks of the orexinergic system in the brains of five microchiropteran species. J Chem Neuroanat 40:256–262. [PubMed: 20654711]

Laux A, Delalande F, Mouheiche J, Stuber D, van Dorsselaer A, Bianchi E, Bezard E, Poisbeau P, Goumon Y. 2012. Localization of endogenous morphine-like compounds in the mouse spinal cord. J Comp Neurol 520:1547–1561. [PubMed: 22102217]

Lu J, Sherman D, Devor M, Saper CB. 2006. A putative flipflop switch for the control of REM sleep. Nature 441: 589–594. [PubMed: 16688184]

Lyamin OI, Manger PR, Ridgway SH, Mukhametov LM, Siegel JM. 2008. Cetacean sleep: an unusual form of mammalian sleep. Neurosci Biobehav Rev 32:1451–1484. [PubMed: 18602158]

Lydic R, Baghdoyan HA. 1993. Pedunculopontine stimulation alters respiration and increases Ach release in the pontine reticular formation. Am J Physiol 264:R544–R554. [PubMed: 8457006]

Manaye KF, Zweig R, Wu D, Hersh LB, De Lacalle S, Saper CB, German DC. 1999. Quantification of cholinergic and select non-cholinergic mesopontine neuronal populations in the human brain. Neuroscience 89:759–770. [PubMed: 10199611]

Manger PR, Ridgway SH, Siegel JM. 2003. The locus coeruleus complex of the bottlenose dolphin (*Tursiops truncatus*) as revealed by tyrosine hydroxylase immunohistochemistry. J Sleep Res 12:149–155. [PubMed: 12753352]

Manger PR, Pillay P, Maseko BC, Bhagwandin A, Gravett N, Moon DJ, Jillani NE, Hemingway J. 2009. Acquisition of the brain of the African elephant (*Loxodonta africana*): perfusion-fixation and dissection. J Neurosci Meth 179: 16–21.

Manger PR, Hemingway J, Haagensen M, Gilissen E. 2010. Cross-sectional area of the elephant corpus callosum: comparison to other Eutherian mammals. Neuroscience 167:815–824. [PubMed: 20206234]

Maseko BC, Bourne JA, Manger PR. 2007. Distribution and morphology of cholinergic, putative catecholaminergic and serotonergic neurons in the brain of the Egyptian Rousette flying fox, *Rousettus aegyptiacus*. J Chem Neuroanat 34:108–127. [PubMed: 17624722]

McLellan WA, Koopman HN, Rommel SA, Read AJ, Potter CW, Nicolas JR, Westgate AJ, Pabst DA. 2002. Ontogenetic allometry and body composition of harbour porpoises (*Phocoena phocoena*) from the western north Atlantic. J Zool Lond 257:457–471.

Michelson KA, Schmitz C, Steinbusch HWM. 2007. The dorsal raphe nucleus from silver stainings to a role in depression. Brain Res Rev 55:329–349. [PubMed: 17316819]

Monti JM. 2011. Serotonin control of sleep-wake behaviour. Sleep Med Rev 15:269–281. [PubMed: 21459634]

Mouton PR, Pakkenberg B, Gundersen HJG, Price DL. 1994. Absolute number and size of pigmented locus coeruleus neurons in young and aged individuals. J Chem Neuroanat 7:185–190. [PubMed: 7848573]

Mukhametov LM. 1987. Unihemispheric slow-wave sleep in the Amazonian dolphin, *Inia geoffrensis*. Neurosci Lett 79:128–132. [PubMed: 3670722]

Mukhametov LM, Supin AYA, Polyakova IG. 1977. Interhemispheric asymmetry of the electroencephalographic sleep pattern in dolphins. Brain Res 134:581–584. [PubMed: 902119]

Oleksenko AI, Chetyrbok IS, Polyakova IG, Mukhametov LM. 1996. Rest and active states in Amazonian dolphins. In: Sokolov VE, editor. The Amazonian dolphin. Moscow: Nauka. p. 257–266.

Patzke N, Spocter MA, Karlsson KÆ, Bertelsen MF, Haagensen M, Chawana R, Streicher S, Kaswera C, Gilissen E, Alagaili AN, Mohammed OB, Reep RL, Bennett NC, Siegel JM, Ihunwo AO, Manger PR. 2015. In contrast to many other mammals, cetaceans have relatively small hippocampi that appear to lack adult neurogenesis. Brain Struct Funct 220:361–383. [PubMed: 24178679]

Petrovic J, Ciric J, Lazic K, Kalauzi A, Saponjic J. 2013. Lesion of the pedunculopontine tegmental nucleus in rat augments cortical activation and disturbs sleep-wake state transitions structure. Exp Neurol 247:562–571. [PubMed: 23481548]

Piskuric NA, Vollmer C, Nurse CA. 2011. Confocal immunofluorescence study of rat aortic body chemoreceptors and associated neurons *in situ* and *in vitro*. J Comp Neurol 519:856–873. [PubMed: 21280041]

Price SA, Bininda-Emonds OR, Gittleman JL. 2005. A complete phylogeny of the whales, dolphins and even-toed hoofed mammals (Cetartiodactyla). Biol Rev 80:445–473. [PubMed: 16094808]

Rae BB. 1965. The food of the common porpoise (*Phocoena phocoena*). Proc Zool Soc Lond 146:114–122.

Rogers JH. 1992. Immunohistochemical markers in rat cortex: colocalization of calretinin and calbindin-D28k with neuropeptides and GABA. Brain Res 587:147–157. [PubMed: 1356060]

Santos MB, Pierce GJ. 2003. The diet of harbour porpoise (*Phocoena phocoena*) in the northeast Atlantic. Oceanogr. Mar Biol Annu Rev 41:355–390.

Saper CB, Fuller PM, Pedersen NP, Lu J, Scammell TE. 2010. Sleep state switching. Neuron 68:1023–1042. [PubMed: 21172606]

Serafetinides EA, Shurley JT, Brooks RE. 1972. Electroencephalogram of the pilot whale, *Globicephala scammoni*, in wakefulness and sleep: lateralization aspects. Intern J Psychobiol 2:129–135.

Siegel JM. 2004. The neurotransmitters of sleep. J Clin Psychiat 65:4–7.

Silver RA, Cull-Candy SG, Takahashi T. 1996. Non-NMDA glutamate receptor occupancy and open probability at the rat cerebellar synapse with single and multiple release sites. J Physiol Lond 494:231–250. [PubMed: 8814618]

Sobel N, Supin AYA, Myslobodsky MS. 1994. Rotational swimming tendencies in the dolphin (*Tursiops truncatus*). Behav Brain Res 65:41–45. [PubMed: 7880453]

Supin AYa, Mukhametov LM. 1986. Some mechanisms of the unihemispheric slow wave sleep in dolphins. In: Sokolov VE, editor. Electrophysiology of sensory systems in marine mammals. Moscow: Nauka. p. 188–207.

Szymusiak R 1995. Magnocellular nuclei of the basal forebrain: substrates of sleep and arousal regulation. Sleep 18:478–500. [PubMed: 7481420]

Syzmusiak R, Steininger T, Alam N, McGinty D. 2001. Preoptic area sleep-regulating mechanisms. Arch Ital Biol 139: 77–92. [PubMed: 11256189]

Takahashi K, Kayama Y, Lin JS, Sakai K. 2010. Locus coeruleus neuronal activity during the sleep-waking cycle in mice. Neuroscience 169:1115–1126. [PubMed: 20542093]

Takakusaki K, Saitoh K, Harada H, Okumura T, Sakamoto T. 2004. Evidence for a role of basal ganglia in the regulation of rapid eye movement sleep by electrical and chemical stimulation for the pedunculopontine tegmental nucleus and the substantia nigra pars reticulata in decerebrate cats. Neuroscience 124:207–220. [PubMed: 14960352]

Thannickal TC, Moore RY, Nienhuis R, Ramanathan L, Gulyani S, Aldrich M, Cornford M, Siegel JM. 2000. Reduced number of hypocretin neurons in human narcolepsy. Neuron 27:469–474. [PubMed: 11055430]

Tobler I 1995. Is sleep fundamentally different between mammalian species? Behav Brain Res 69:35–41. [PubMed: 7546316]

Walløe S, Eriksen N, Dabelsteen T, Pakkenberg B. 2010. A neurological comparative study of the harp seal (*Pagophilus groenlandicus*) and harbour porpoise (*Phocoena phocoena*) brain. Anat Rec 293:2129–2135.

West MJ, Slomianka L, Gundersen HJ. 1991. Unbiased stereological estimation of the total number of neurons in the subdivisions of the rat hippocampus using the optical fractionator. Anat Rec 231:482–497. [PubMed: 1793176]

Wilson RB. 1933. The anatomy of the brain of the whale (*Balaenoptera sulfurea*). J Comp Neurol 58:419–480.

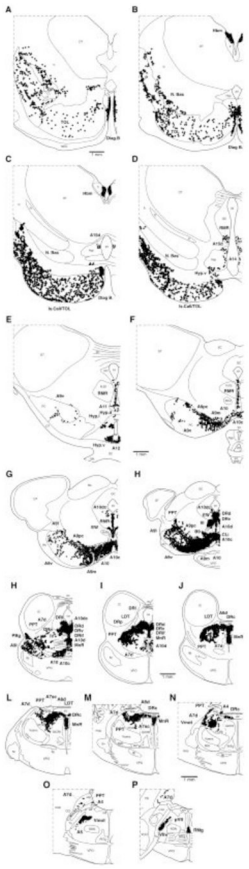

Figure 1.

A–P: Diagrammatic reconstruction of a series of coronal sections through the basal forebrain, diencephalon, midbrain, and pons of the harbor porpoise brain illustrating the location of neurons immunohistochemically reactive for choline acetyltransferase (ChAT; circles), tyrosine hydroxylase (TH; squares), and serotonin (stars). Each symbol represents a single neuron. The outlines of the architectonic regions were drawn using Nissl and myelin stain and immunoreactive neurons marked on the drawings from one animal. A represents the most rostral section, and P the most caudal. Each panel is approximately 4 mm apart. For abbreviations, see list.

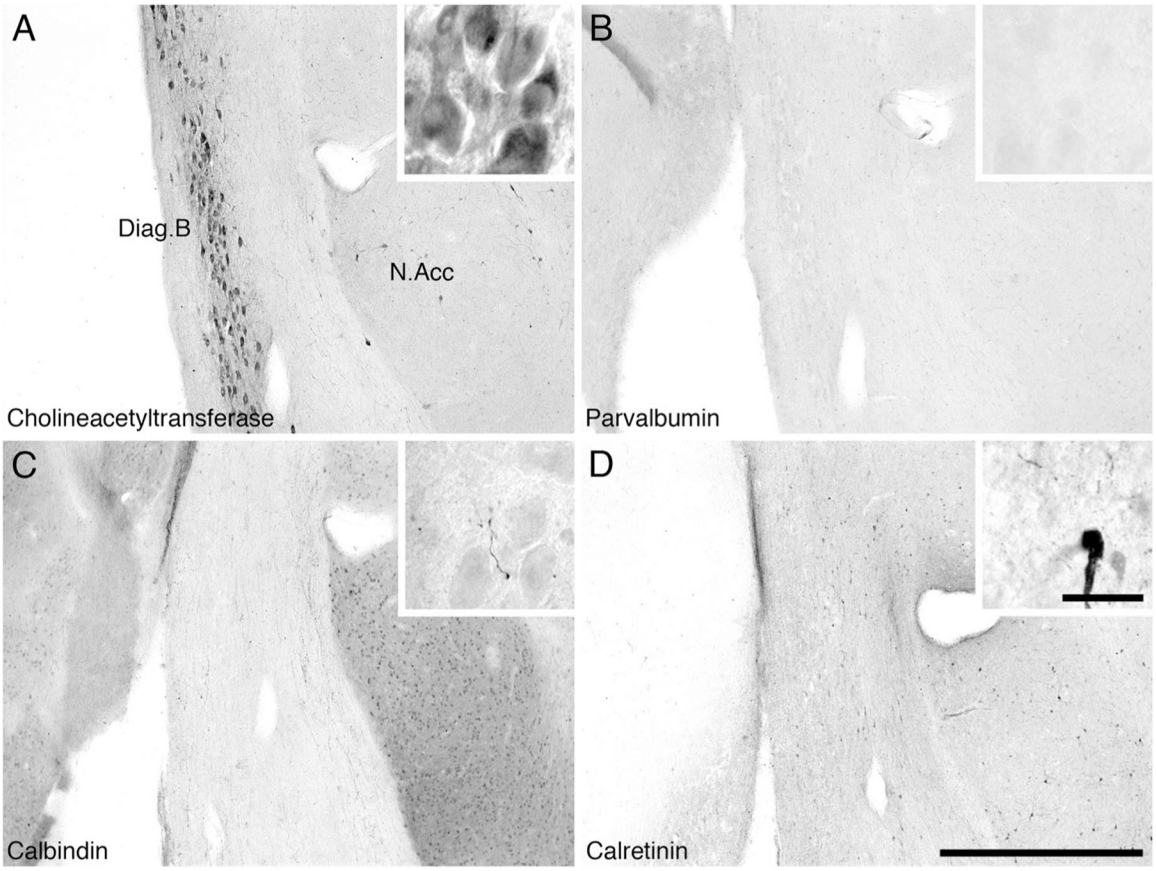

Figure 2.

Low (main image) and high (inset) magnification photomicrographs of the region of the diagonal band of Broca (Diag. B). **A:** Neurons immunoreactive for cholineacetyltransferase showing the diagonal band of Broca (**Diag.B**) and the nucleus accumbens (N. Acc). **B:** Parvalbumin immunoreactivity. Note the very low density of parvalbumin-immunoreactive structures in the diagonal band. **C:** Calbindin immunoreactivity. Note the lack of reactivity in the diagonal band, but strong reactivity in the nucleus accumbens. **D:** Calretinin immunoreactivity. Note the low density of cells and terminal networks in the diagonal band and nucleus accumbens. In all images medial is to the left and dorsal to the top. Scale bar = 1,000 μm in D (applies to A–D); 50 μm in inset to D (applies to insets in A–D).

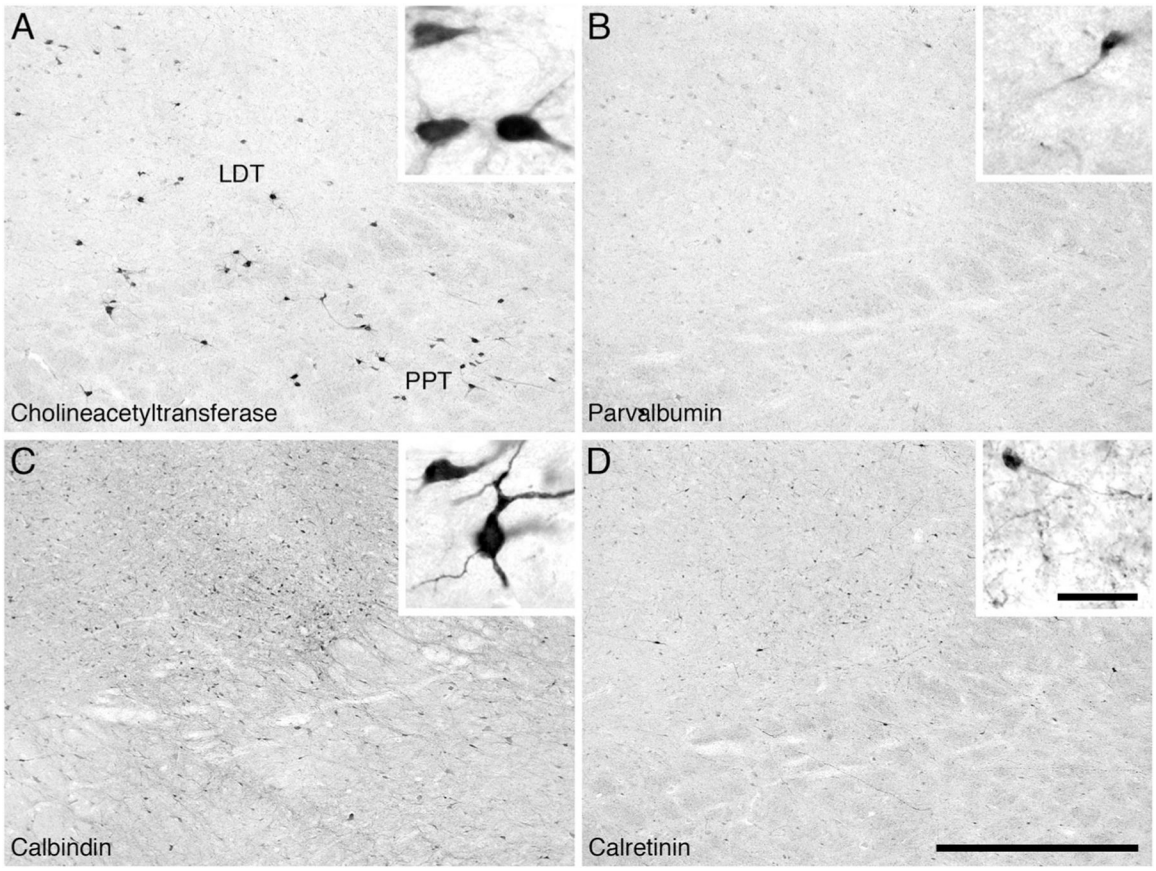

Figure 3.

Low (main image) and high (inset) magnification photomicrographs of the region of the pontine cholinergic nuclei. **A:** Neurons immunoreactive for cholineacetyltransferase showing the laterodorsal tegmental (LDT) and pedunculopontine tegmental (PPT) nuclei. **B:** Parvalbumin immunoreactivity. Note the low density of parvalbumin-immunoreactive structures in both the LDT and PPT. **C:** Calbindin immunoreactivity. Note the high density of cells and terminals in the region of the LDT and the moderate density of immunoreactive cells and terminals in the region of the PPT. **D:** Calretinin immunoreactivity. Note the high to moderate density of cells and terminals in the region of the LDT and the moderate to low density of immunoreactive cells and terminals in the region of the PPT. In all images medial is to the left and dorsal to the top. Scale bar = 1,000 μm in D (applies to A–D); 50 μm in inset to D (applies to insets in A–D).

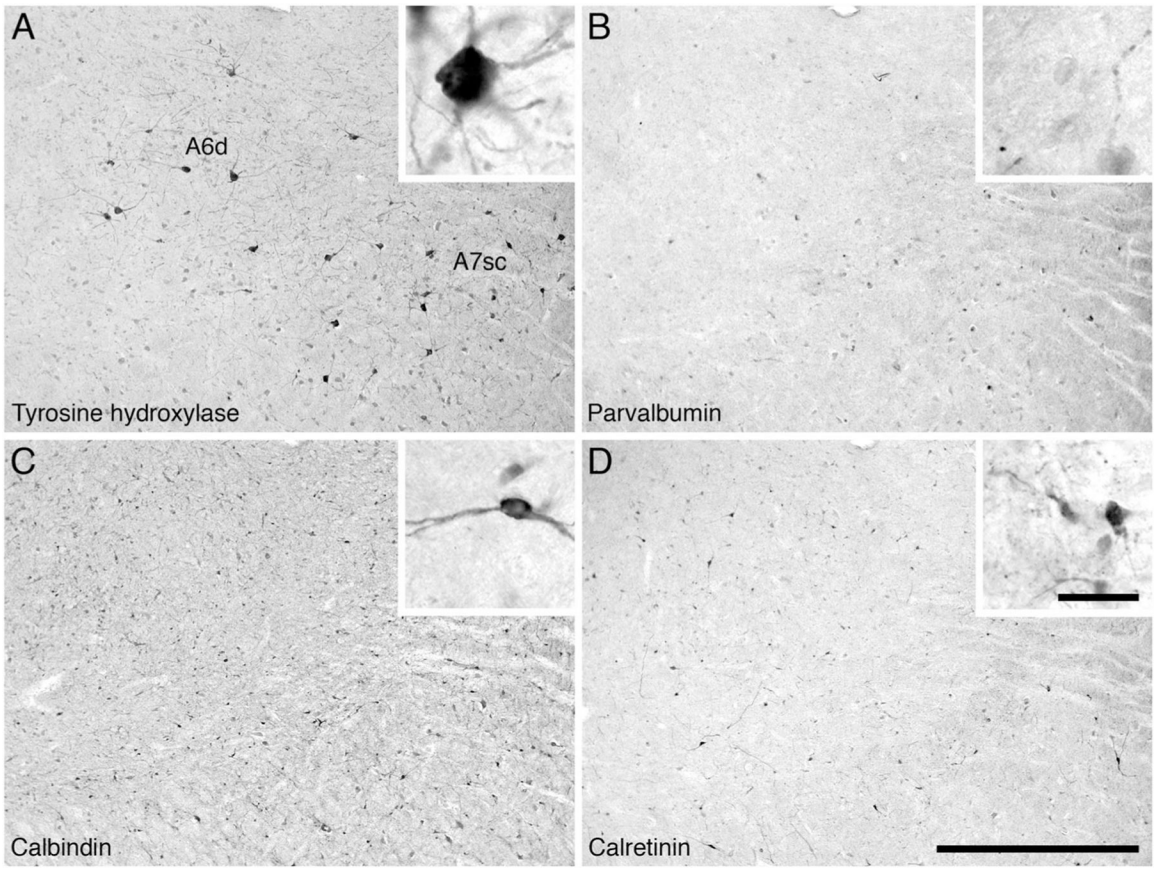

Figure 4.

Low (main image) and high (inset) magnification photomicrographs of the region of the locus coeruleus complex. **A:** Neurons immunoreactive for tyrosine hydroxylase showing the diffuse portion of the locus coeruleus (A6d) and the compact portion of the subcoeruleus (A7sc). **B:** Parvalbumin immunoreactivity. Note the low density of parvalbumin-immunoreactive structures in both the A6d and A7sc. **C:** Calbindin immunoreactivity. Note the high density of cells and terminals in the region of both the A6d and A7sc. **D:** Calretinin immunoreactivity. Note the moderate density of cells and terminals in the region of both the A6d and A7sc. In all images medial is to the left and dorsal to the top. Scale bar = 1,000 μm in D (applies to A–D); 50 μm in inset to D (applies to insets in A–D).

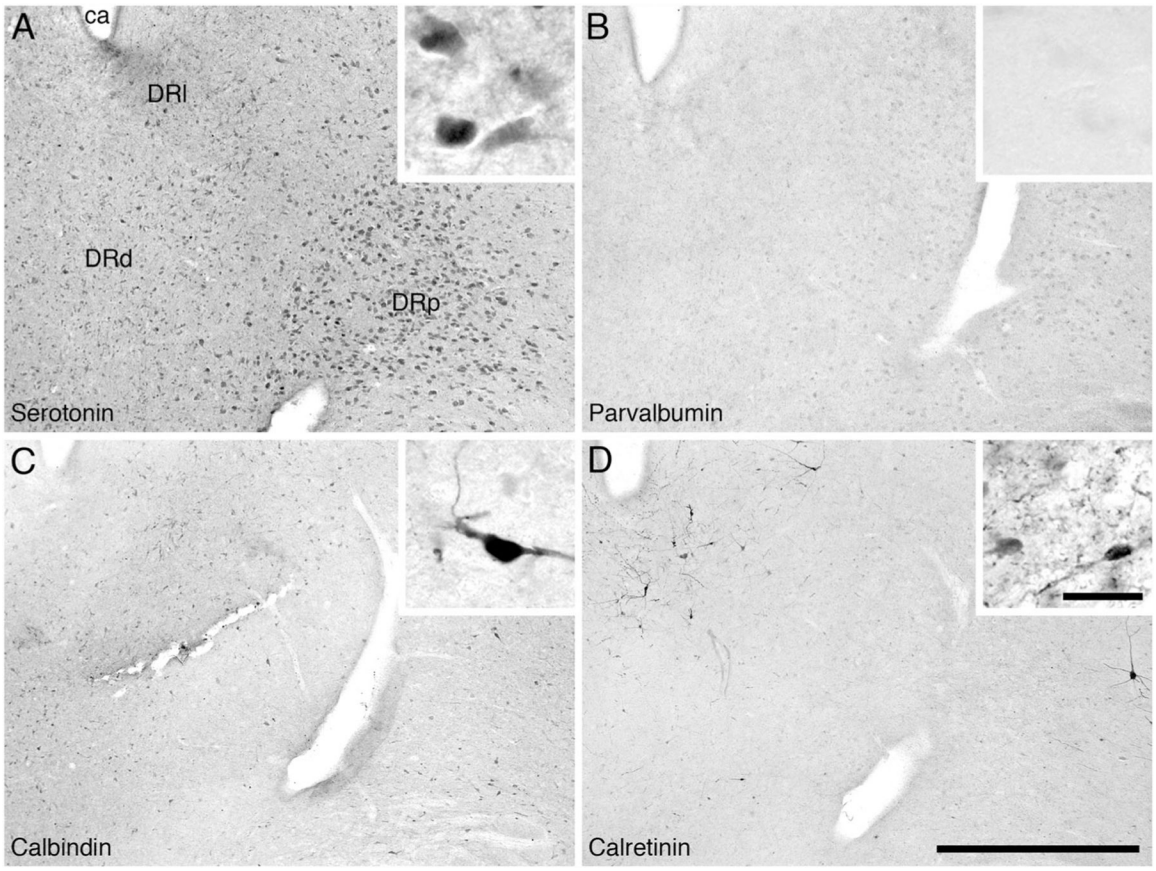

Figure 5.

Low (main image) and high (inset) magnification photomicrographs of the region of the dorsal raphe nuclear complex. **A:** Neurons immunoreactive for serotonin showing the dorsal (DRd), lateral (DRl) and peripheral (DRp) subdivisions. Note the very high density and number of serotonergic cells in the DRp. **B:** Parvalbumin immunoreactivity. Note the absence of parvalbumin-immunoreactive structures in this region. **C:** Calbindin immunoreactivity. Note the moderate density of cells and terminals in this region. **D:** Calretinin immunoreactivity. Note the low density of cells and terminals in the region of the DRd and DRp, but the moderate to high density of cells and terminals in the region of the DRl. In all images medial is to the left and dorsal to the top. Scale bar = 1,000 μm in D (applies to A–D); 50 μm in inset to D (applies to insets in A–D).

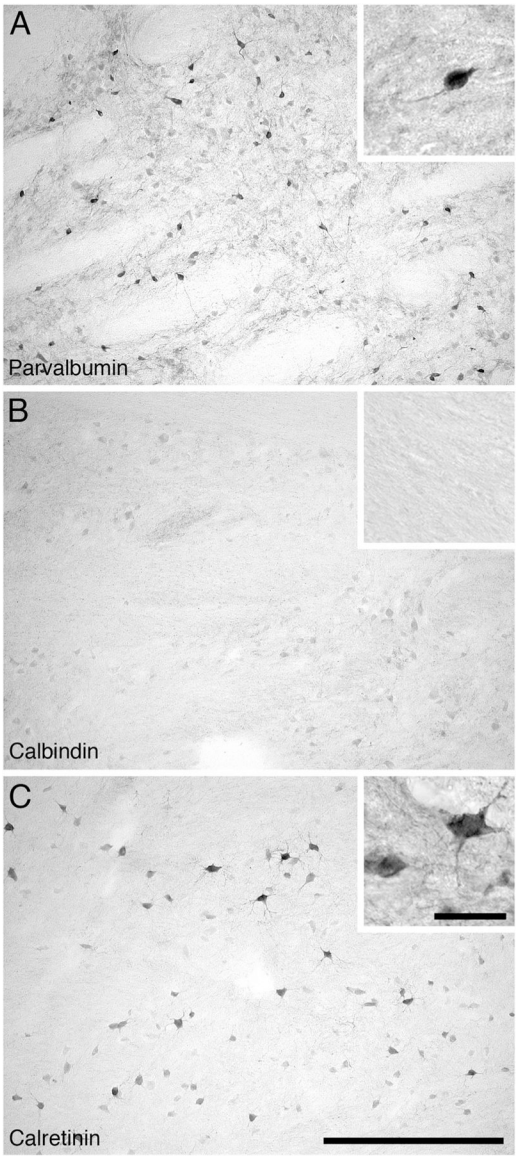

Figure 6.

Low (main image) and high (inset) magnification photomicrographs of the thalamic reticular nucleus of the harbor porpoise following immunohistochemical staining for parvalbumin (**A**), calbindin (**B**), and calretinin (**C**). While the parvalbumin-immunopositive neurons, and the lack of calbindin-immunopositive neurons is similar to that reported for other mammals, the large and highly branched calretin-inimmunopositive neurons are unusual. In all images medial is to the left and dorsal to the top. Scale bar = 500 μm in D (applies to A–C); 50 μm in inset to C (applies to insets in A–C).

TABLE 1.

Sources and Dilutions of Antibodies Used in This Study

Antibody	Host	Immunogen	Manufacturer	Cat. No.	Reference	Dilution	RRID
ChAT	Goat	Human placental enzyme	Merck-Millipore	AB144P	Laux et al., 2012; Kaiser et al., 2011	1:2,500	AB_2079751
TH	Rabbit	Purified tyrosine hydroxlase from rat adrenal	Merck-Millipore	AB151	Piskuric et al., 2011	1:7,500	AB_10000323
5-HT	Rabbit	The antigen used in the production of this antiserum is serotonin covalently bound to bovine thyroglobulin with carbodiimide	Merck-Millipore	AB938	Not available	1:7,500	Not available
PV	Rabbit	Rat muscle parvalbumin	Swant	PV28	Hirano et al., 2011	1:10,000	AB_10000343
CB	Rabbit	Rat recombinant calbindin D-28k	Swant	CB38a	Bunce et al., 2013	1:10,000	AB_10000340
CR	Rabbit	Recombinant human calretinin containing a 6-his tag at the N-terminal	Swant	7699/3H	Adrio et al., 2011	1:10,000	AB_10000321

For abbreviations, see list.

TABLE 2.

Stereological Parameters Used for Estimating Neuron Numbers in the Harbor Porpoise

Nuclei examined	Counting frame size (μm)	Sampling grid size ((μm)	Disector height (μm)	Cut thickness (μm)	Average mounted thickness (urn)	Vertical guard zones (top and bottom,μm)	Section interval	No. of sections	No. of sampling sites	Average CE (Gundersen m = 0)	Average CE (Gundersen m = 1)
LDT (ChAT+)	200 × 200	200 × 200	15	50	33.3	5	10	14	1,389	0.05	0.04
PPT (ChAT+)	200 × 200	800 × 800	15	50	25.7	5	10	21	396	0.08	0.07
LC (TH+)	150 × 150	700 × 700	15	50	26.8	5	10	25	600	0.08	0.08

Abbreviations: LDT, laterodorsal tegmental nucleus; PPT, pedunculopontine tegmental nucleus; LC, locus coeruleus complex; ChAT+, neurons immunopositive for choline acetyltransferase; TH+, neurons immunopositive for tyrosine hydroxylase.

TABLE 3.

Stereological Results for Neuron Numbers, Volume, and Area in the Harbor Porpoise

Nuclei examined	Total estimated population using mean section thickness	Average estimated cell volume (μm^3)	Average estimated cell area (μm^2)
LDT (ChAT+)	15,642	2,790.14	1,136.20
PPT (ChAT+)	111,134	2,648.00	1,196.26
LC (TH+)	122,878	1,624.16	647.99

Abbreviations: LDT, laterodorsal tegmental nucleus; PPT, pedunculopontine tegmental nucleus; LC, locus coeruleus complex; ChAT+, neurons immunopositive for choline acetyltransferase; TH+, neurons immunopositive for tyrosine hydroxylase.

TABLE 4.

Density of Neurons and Terminal Networks of the Calcium Binding Proteins Calbindin (CB), Calretinin (CR), and Parvalbumin (PV) in Relation to Various Sleep–Wake Nuclei in the Brain of the Harbor Porpoise[1]

	Calbindin		Calretinin		Parvalbumin	
Sleep-related nuclei	**Neurons**	**Terminal networks**	**Neurons**	**Terminal networks**	**Neurons**	**Terminal networks**
Cholinergic						
Diagonal band of Broca	++	+	+	++	+	+
Islands of Calleja and olfactory tubercle	+++	+	+	+	+	−
Nucleus basalis	++	−	++	+	++	−
Pedunculopontine tegmental nucleus	+	+++	+	+	−	+
Laterodorsal tegmental nucleus	++	+ +	+	+	−	+
Catecholaminergic						
Compact subcoeruleus (A7sc)	+++	+++	+	++	+	+
Diffuse subcoeruleus (A7d)	++	++	+	++	+	+
Diffuse locus coeruleus (A6d)	++	++	++	++	+	+
Serotonergic						
Dorsal raphe, interfascicular (DRif)	+	+	−	−	−	−
Dorsal raphe, ventral (DRv)	++	+	+	++	+	+
Dorsal raphe, dorsal (DRd)	++	++	++	++	+	+
Dorsal raphe, lateral (DRl)	++	+++	+++	+++	+	+
Dorsal raphe, peripheral (DRp)	+++	++	+++	+++	+	+
Dorsal raphe, caudal (DRc)	++	++	+	++	−	++
Orexinergic						
Main magnocellular cluster	++	++	++	+	+	−
Optic tract cluster	+	++	+	−	−	−
Zona incerta cluster	++	−	+	−	+	−
Medial parvocellular cluster	++	++	++	+	+	−
Thalamic reticular nucleus	+	+	+++	++	+++	+++

[1]−, absence; +, low density; ++, moderate density; +++, high density.